Discontinuous Galerkin method for Krause's consensus models and pressureless Euler equations[1]

Yang Yang[2], Dongming Wei[3] and Chi-Wang Shu[4]

Abstract

In this paper, we apply discontinuous Galerkin (DG) methods to solve two model equations: Krause's consensus models and pressureless Euler equations. These two models are used to describe the collisions of particles, and the distributions can be identified as density functions. If the particles are placed at a single point, then the density function turns out to be a δ-function and is difficult to be well approximated numerically. In this paper, we use DG method to approximate such a singularity and demonstrate the good performance of the scheme. Since the density functions are always positive, we apply a positivity-preserving limiter to them. Moreover, for pressureless Euler equations, the velocity satisfies the maximum principle. We also construct special limiters to fulfill this requirement.

Keywords: δ-singularities, discontinuous Galerkin method, Krause's model, pressureless gas, positivity preserving, symmetry preserving, maximum principle.

[1]Research supported by DOE grant DE-FG02-08ER25863 and NSF grant DMS-1112700.

[2]Division of Applied Mathematics, Brown University, Providence, RI 02912. E-mail: yang_yang@brown.edu

[3]Division of Applied Mathematics, Brown University, Providence, RI 02912. Current address: PNC Financial Services Group, Inc., New York, New York. E-mail:weidongmmm@hotmail.com

[4]Division of Applied Mathematics, Brown University, Providence, RI 02912. E-mail: shu@dam.brown.edu

1 Introduction

In this paper, we apply discontinuous Galerkin (DG) methods to solve the hyperbolic conservation law

$$\begin{aligned} &\mathbf{u}_t + \nabla \cdot \mathbf{f}(\mathbf{u}) = 0, && (\mathbf{x}, t) \in \mathbb{R}^d \times (0, T], \\ &\mathbf{u}(\mathbf{x}, 0) = \mathbf{u}_0(\mathbf{x}), && \mathbf{x} \in \mathbb{R}^d, \end{aligned} \tag{1.1}$$

where d is the spatial dimension and the exact solution $\mathbf{u}(\mathbf{x}, t)$ contains δ-singularities. Such problems appear often in applications and are difficult to be well approximated numerically. Most of the previous techniques are designed to modify the singularities with smooth kernels in some narrow region, and hence may smear such singularities severely, leading to large errors in the approximation. On the other hand, the DG methods rely on weak formulations and can solve such problems directly, leading to very accurate results. The first work on approximating δ-singularities with DG methods is [24], in which the authors proved the superconvergence results for linear hyperbolic equations with singular initial data and singular source terms. Moreover, several numerical examples were also given in [24] to demonstrate the advantages of the DG scheme in approximating δ-singularities for both linear and nonlinear hyperbolic equations. In this paper, we extend the work in [24] and consider applications to two model equations: Krause's consensus models and pressureless Euler equations.

The DG method, first introduced by Reed and Hill in 1973 [19], was extended to solve scalar linear hyperbolic equations by Johnson and Pitkäranta [18]. Later, Cockburn et al. studied Runge-Kutta discontinuous Galerkin (RKDG) methods for hyperbolic conservation laws [14, 12, 13, 15]. Recently, in [25], genuinely maximum-principle-satisfying high order DG schemes for scalar equations and two-dimensional incompressible flows in vorticity-streamfunction formulation have been constructed. Subsequently, positivity-preserving high order DG schemes for compressible Euler equations were given in [26]. In this paper, we extend the ideas in [25, 26] to construct bound-preserving high order DG schemes for the Krause's consensus models and pressureless Euler equations.

For the first example, we discuss the following Krause's consensus model equation

$$\begin{array}{ll} \rho_t + F_x = 0, & x \in [0,1], t > 0, \\ \rho(x,0) = \rho_0(x), & t > 0, \end{array} \tag{1.2}$$

where ρ is the density function, which is always positive. The flux F is given by

$$F(x,t) = v(x,t)\rho(x,t),$$

and the velocity v is defined by

$$v(x,t) = \int_0^1 (y-x)\xi(y-x)\rho(y,t)dy,$$

where $0 \leq \xi(x) \leq 1$ is supported on a ball centered at zero with radius R. In [7], Canuto et al. investigated the discretized version of the PDE and proved that when the time t tends to infinity, the density function ρ will converge to some isolated δ-singularities, and the distance between any two of these δ-singularities cannot be less than R. Some computational results are shown in [7] based on a first order finite volume method. For two dimensions, if the initial density is rotationally invariant, the limit density should also be rotationally invariant, and hence can only be a single delta located at the center. However, direct computations on rectangle meshes yield more than one delta singularity for sufficiently small R. This is because the meshes are not invariant under rotation. In this paper, following the idea in [9, 10], we construct a special mesh to obtain symmetry and convergence to physically relevant solutions. Computational results are given to demonstrate the advantages of high order DG schemes.

For the second example, we discuss the pressureless Euler equation

$$\begin{array}{l} \rho_t + \nabla \cdot (\rho \mathbf{u}) = 0, \\ (\rho \mathbf{u})_t + \nabla \cdot (\rho \mathbf{u} \otimes \mathbf{u}) = 0, \end{array} \tag{1.3}$$

where ρ is the density function and $\mathbf{u}$ is the velocity. Pressureless Euler equations in one space dimension have been analyzed at the theoretical level intensively, e.g. [2, 3, 6, 8, 16]. Some numerical methods have also been studied by several authors [4, 1, 11, 5]. In [4], only first and second order numerical schemes were considered. Except for those in [4], no other

methods seem to have been designed to solve the equation (1.3) directly. In [5], the authors added an artificial viscosity and built a diffusive scheme. In [11], the authors applied the sticky particle methods to the equation and showed the approximation satisfies the original system within a certain residual. In [1], the authors introduced a new variable and added one more equation to the system, leading to more computational cost. In this paper, we consider high order DG scheme and approximate the equation without modification. Physically, the density ρ is positive and the velocity $\mathbf{u}$ satisfies a maximum principle. We extend the idea in [26] and construct suitable limiters to fulfill these two requirements while maintaining high order accuracy. Moreover, numerical evidences also demonstrate that the scheme is good for approximations in the presence of vacuum. Finally, our scheme works well in two dimensions. To the authors' knowledge, few works in the literature focus on the computational aspects of two dimensional equations, although some theoretical results can be found in [20, 21]. It appears that complete existence and uniqueness results are not available. Therefore, our scheme should be a good tool to study two-dimensional pressureless Euler equations and other similar equations.

The organization of this paper is as follows. In section 2, we present some preliminaries, including the implementation of the DG scheme, the foundation of the limiters, and high order time discretizations. In sections 3 and 4, we discuss the two models in detail, and numerical evidences are given to demonstrate the advantages of the DG methods. Finally, we will end in section 5 with some concluding remarks and remarks for future work.

2 Preliminaries

In this section, we consider one space dimension only.

2.1 The DG scheme in one space dimension

First, we divide the computational domain $\Omega = [0, 1]$ into N cells

$$0 = x_{\frac{1}{2}} < x_{\frac{3}{2}} < \cdots < x_{N+\frac{1}{2}} = 1,$$

and denote

$$I_j = \left(x_{j-\frac{1}{2}}, x_{j+\frac{1}{2}}\right)$$

as the cells. For simplicity, we consider uniform mesh in this paper, and denote by Δx the size of each cell.

Next, we define

$$V_h = \left\{\mathbf{v} : \text{each of its components } v_i|_{I_j} \in \mathcal{P}^k(I_j), j = 1, \cdots, N\right\}$$

as the finite element space, where $\mathcal{P}^k(I_j)$ denotes the space of polynomials in I_j of degree at most k. The DG scheme for (1.1) is the following: find $\mathbf{u}_h \in V_h$, such that for any $\mathbf{v}_h \in V_h$

$$((\mathbf{u}_h)_t, \mathbf{v}_h)_j = (\mathbf{f}(\mathbf{u}_h), (\mathbf{v}_h)_x)_j + \hat{\mathbf{f}}_{j-\frac{1}{2}}\mathbf{v}_h^+|_{j-\frac{1}{2}} - \hat{\mathbf{f}}_{j+\frac{1}{2}}\mathbf{v}_h^-|_{j+\frac{1}{2}}, \tag{2.1}$$

where $(\mathbf{w}, \mathbf{v})_j = \int_{I_j} \mathbf{w}\mathbf{v}dx$, and $\mathbf{v}_h^-|_{j+\frac{1}{2}} = \mathbf{v}_h(x^-_{j+\frac{1}{2}})$ denotes the left limit of the vector $\mathbf{v}_h$ at $x_{j+\frac{1}{2}}$. Likewise for $\mathbf{v}_h^+$. Moreover, the numerical flux $\hat{\mathbf{f}}$ is a single valued vector defined at the cell interfaces and in general depends on the values of the numerical solution $\mathbf{u}_h$ from both sides of the interfaces

$$\hat{\mathbf{f}}_{i+\frac{1}{2}} = \hat{\mathbf{f}}(\mathbf{u}_h(x^-_{i+\frac{1}{2}}), \mathbf{u}_h(x^+_{i+\frac{1}{2}})).$$

In general, for scalar equations, we use monotone fluxes.

2.2 Limiters

In this subsection, we use Euler-forward for time discretization and briefly discuss the construction of bound-preserving limiters [27]. For the two model problems (1.2) and (1.3), direct usage of high order DG methods results in the appearance of negative densities. Since the problems are ill-posed for negative densities, the code may blow up once negative densities appear. Therefore, we would need to use bound-preserving limiter to keep the positivity of the density. We denote $\mathbf{u}_j^n$ and $\overline{\mathbf{u}}_j^n$ to be the numerical solution and its cell average at time level n in cell I_j. For simplicity, throughout the paper, if we consider generic numerical solution on the whole computational domain Ω, then the subscript j will be omitted.

Suppose the exact solution of equation (1.1) is in some convex set G, we are interested in constructing numerical solutions which are also in G. The whole precess can be divided into three steps.

2.2.1 First order scheme

In the first step, we consider a first order scheme

$$\begin{aligned}\mathbf{u}_j^{n+1} &= \mathbf{u}_j^n + \lambda\left(\hat{\mathbf{f}}\left(\mathbf{u}_{j-1}^n, \mathbf{u}_j^n\right) - \hat{\mathbf{f}}\left(\mathbf{u}_j^n, \mathbf{u}_{j+1}^n\right)\right)\\ &= \frac{1}{2}\left(\mathbf{u}_j^n + 2\lambda\hat{\mathbf{f}}\left(\mathbf{u}_{j-1}^n, \mathbf{u}_j^n\right)\right) + \frac{1}{2}\left(\mathbf{u}_j^n - 2\lambda\hat{\mathbf{f}}\left(\mathbf{u}_j^n, \mathbf{u}_{j+1}^n\right)\right)\\ &= \frac{1}{2}\mathbf{H}_1\left(\mathbf{u}_{j-1}^n, \mathbf{u}_j^n, 2\lambda\right) + \frac{1}{2}\mathbf{H}_2\left(\mathbf{u}_j^n, \mathbf{u}_{j+1}^n, 2\lambda\right),\end{aligned} \tag{2.2}$$

where

$$\mathbf{H}_1(\mathbf{u}, \mathbf{v}, c) = \mathbf{v} + c\,\hat{\mathbf{f}}(\mathbf{u}, \mathbf{v}), \quad \mathbf{H}_2(\mathbf{u}, \mathbf{v}, c) = \mathbf{u} - c\,\hat{\mathbf{f}}(\mathbf{u}, \mathbf{v}). \tag{2.3}$$

Here $\mathbf{u}_j^n = \overline{\mathbf{u}}_j^n$ is a constant in each cell I_j, and $\lambda = \frac{\Delta t}{\Delta x}$ is the ratio of time and space mesh sizes. For many two-point first order numerical fluxes, we can prove the following property.

Property 2.1 *Suppose G is a convex set and $\mathbf{u}, \mathbf{v} \in G$, then there exists a positive constant $C_\star$, such that, for any $0 < c < C_\star$, we have $\mathbf{H}_1(\mathbf{u}, \mathbf{v}, c), \mathbf{H}_2(\mathbf{u}, \mathbf{v}, c) \in G$.*

Based on the above property, we can easily obtain that, under the CFL condition $\lambda < \frac{C_\star}{2}$, $\mathbf{u}^n \in G$ implies $\mathbf{u}^{n+1} \in G$.

2.2.2 High order schemes

Next, we consider high order schemes and assume $\mathbf{u}^n \in G$. By taking the test function $\mathbf{v}_h = \mathbf{1}$ in equation (2.1), we have

$$\bar{\mathbf{u}}_j^{n+1} = \bar{\mathbf{u}}_j^n + \lambda\left(\hat{\mathbf{f}}(\mathbf{u}_{j-\frac{1}{2}}^-, \mathbf{u}_{j-\frac{1}{2}}^+) - \hat{\mathbf{f}}(\mathbf{u}_{j+\frac{1}{2}}^-, \mathbf{u}_{j+\frac{1}{2}}^+)\right). \tag{2.4}$$

Let α_i be the Legendre Gauss-Lobatto quadrature weights for the interval $[-\frac{1}{2}, \frac{1}{2}]$ such that $\sum_{i=0}^{M} \alpha_i = 1$, with $2M - 3 \geq k$, and denote the corresponding Gauss-Lobatto points in cell

I_j as $\{x_i^j\}$, then the Gauss-Lobatto quadrature yields

$$\bar{\mathbf{u}}_j^n = \sum_{i=0}^{M} \alpha_i \mathbf{u}_j^n(x_i^j).$$

Clearly, $\mathbf{u}_j^n(x_0^j) = \mathbf{u}^+_{j-\frac{1}{2}}$ and $\mathbf{u}_j^n(x_M^j) = \mathbf{u}^-_{j+\frac{1}{2}}$. Therefore,

$$\begin{aligned}
\bar{\mathbf{u}}_j^{n+1} &= \sum_{i=0}^{M} \alpha_i \mathbf{u}_j^n(x_i^j) + \lambda \left(\hat{\mathbf{f}}(\mathbf{u}^-_{j-\frac{1}{2}}, \mathbf{u}^+_{j-\frac{1}{2}}) - \hat{\mathbf{f}}(\mathbf{u}^-_{j+\frac{1}{2}}, \mathbf{u}^+_{j+\frac{1}{2}}) \right) \\
&= \sum_{i=1}^{M-1} \alpha_i \mathbf{u}_j^n(x_i^j) + \alpha_0 \mathbf{H}_1 \left(\mathbf{u}^-_{j-\frac{1}{2}}, \mathbf{u}^+_{j-\frac{1}{2}}, \frac{\lambda}{\alpha_0} \right) + \alpha_M \mathbf{H}_2 \left(\mathbf{u}^-_{j+\frac{1}{2}}, \mathbf{u}^+_{j+\frac{1}{2}}, \frac{\lambda}{\alpha_M} \right).
\end{aligned}$$

If the numerical flux satisfies Property 2.1, we have

$$\mathbf{H}_1 \left(\mathbf{u}^-_{j-\frac{1}{2}}, \mathbf{u}^+_{j-\frac{1}{2}}, \frac{\lambda}{\alpha_0} \right) \in G, \qquad \mathbf{H}_2 \left(\mathbf{u}^-_{j+\frac{1}{2}}, \mathbf{u}^+_{j+\frac{1}{2}}, \frac{\lambda}{\alpha_M} \right) \in G,$$

provided the suitable CFL condition $\lambda < \alpha_0 C_\star$ is satisfied. Here, we have used the fact that $\alpha_0 = \alpha_M$. Since $\mathbf{u}_j^n(x_i^j) \in G$ and G is a convex set, we have $\bar{\mathbf{u}}_j^{n+1} \in G$.

Finally, we can modify the numerical solution through the simple scaling limiter $\tilde{\mathbf{u}}_j^{n+1} = \bar{\mathbf{u}}_j^{n+1} + \theta \left(\mathbf{u}_j^{n+1} - \bar{\mathbf{u}}_j^{n+1} \right)$. By taking suitable $\theta \in [0, 1]$, we have $\tilde{\mathbf{u}}_j^{n+1} \in G$, and $\tilde{\mathbf{u}}_j^{n+1}$ is used as the numerical solution at time level $n+1$. For scalar equations, we can prove that this modification does not affect the high order accuracy of the original solution $\mathbf{u}_j^{n+1}$ [27]. For systems, this modification might lead to slight degeneration of accuracy under certain circumstances, see [28] for a discussion, and also Example 1 in Sections 4.3.1 and 4.3.2 for the numerical experiment results.

2.3 High order time discretizations

We will use strong stability preserving (SSP) high order time discretizations to solve the ODE system $\mathbf{u}_t = \mathbf{L}\mathbf{u}$. More details of these time discretizations can be found in [23, 22, 17]. In this paper, we use the third order SSP Runge-Kutta method [23]

$$\begin{aligned}
\mathbf{u}^{(1)} &= \mathbf{u}^n + \Delta t \mathbf{L}(\mathbf{u}^n), \\
\mathbf{u}^{(2)} &= \frac{3}{4}\mathbf{u}^n + \frac{1}{4}\left(\mathbf{u}^{(1)} + \Delta t \mathbf{L}(\mathbf{u}^{(1)}) \right), \qquad (2.5)
\end{aligned}$$

$$\mathbf{u}^{n+1} = \frac{1}{3}\mathbf{u}^n + \frac{2}{3}\left(\mathbf{u}^{(2)} + \Delta t \mathbf{L}(\mathbf{u}^{(2)})\right),$$

and the third order SSP multi-step method [22]

$$\mathbf{u}^{n+1} = \frac{16}{27}\left(\mathbf{u}^n + 3\Delta t \mathbf{L}(\mathbf{u}^n)\right) + \frac{11}{27}\left(\mathbf{u}^{n-3} + \frac{12}{11}\Delta t \mathbf{L}(\mathbf{u}^{n-3})\right). \tag{2.6}$$

Since a SSP time discretization is a convex combination of Euler forward, by using the limiter mentioned in section 2.2, the numerical solution obtained from the full scheme is also in G.

3 Krause's consensus models

In this section we apply DG methods to Krause's consensus models, extending the results in [7].

3.1 Positivity-preserving high order schemes

We consider equation (1.2) in more detail. For this model, we define $G = \{\rho : \rho > 0\}$. Clearly, G is a convex set.

3.1.1 First order scheme

We start with the following first order scheme

$$\rho_j^{n+1} = \rho_j^n + \lambda\left(v_{j-\frac{1}{2}} h(\rho_{j-1}^n, \rho_j^n) - v_{j+\frac{1}{2}} h(\rho_j^n, \rho_{j+1}^n)\right), \tag{3.1}$$

where $h(\cdot,\cdot)$ is a numerical flux, and $\rho_j^n = \overline{\rho}_j^n$ is the numerical approximation to the exact solution in cell I_j at time level n, with $\overline{\rho}_j^n$ being its cell average. Moreover, $v_{j-\frac{1}{2}}$ is the numerical velocity at the interface $x_{j-\frac{1}{2}}$, given by

$$v_{j-\frac{1}{2}} = \sum_{i=1}^{N} \int_{I_i} (y - x_{j-\frac{1}{2}}) \xi(y - x_{j-\frac{1}{2}}) \rho_i^n(y) dy.$$

For this model, we use an upwind flux, i.e.

$$vh(u,w) = \begin{cases} vu & v \geq 0, \\ vw & v < 0, \end{cases}$$

and define H_1 and H_2 as

$$H_1(u,w,c) = w + cvh(u,w), \quad H_2(u,w,c) = u - cvh(u,w).$$

Then the scheme (3.1) can be written as

$$\rho_j^{n+1} = \frac{1}{2}H_1(\rho_{j-1}^n, \rho_j^n, 2\lambda) + \frac{1}{2}H_2(\rho_j^n, \rho_{j+1}^n, 2\lambda),$$

which further yields the following lemma.

Lemma 3.1 *Suppose $\rho^n > 0$ in (3.1), then under the CFL condition*

$$\max_j |v_{j-\frac{1}{2}}|\lambda < \frac{1}{2},$$

we have $\rho^{n+1} > 0$.

Proof: We consider $H_1(\rho_{j-1}^n, \rho_j^n, 2\lambda)$ first. If $v_{j-\frac{1}{2}} < 0$, then

$$H_1(\rho_{j-1}^n, \rho_j^n, 2\lambda) = \rho_j^n + 2\lambda v_{j-\frac{1}{2}} h(\rho_{j-1}^n, \rho_j^n) = (1 + 2\lambda v_{j-\frac{1}{2}})\rho_j^n > 0.$$

On the other hand, if $v_{j-\frac{1}{2}} \geq 0$, then

$$H_1(\rho_{j-1}^n, \rho_j^n, 2\lambda) = \rho_j^n + 2\lambda v_{j-\frac{1}{2}} h(\rho_{j-1}^n, \rho_j^n) = \rho_j^n + 2\lambda v_{j-\frac{1}{2}} \rho_{j-1}^n > 0.$$

Similarly, we have

$$H_2(\rho_j^n, \rho_{j+1}^n, 2\lambda) = \rho_j^n - 2\lambda v_{j+\frac{1}{2}} h(\rho_j^n, \rho_{j+1}^n) > 0.$$

Therefore,

$$\rho_j^{n+1} = \frac{1}{2}H_1(\rho_{j-1}^n, \rho_j^n, 2\lambda) + \frac{1}{2}H_2(\rho_j^n, \rho_{j+1}^n, 2\lambda) > 0. \quad \square$$

3.1.2 High order schemes

Now, we proceed to the high order schemes and the scheme satisfied by the numerical cell averages can be written as

$$\overline{\rho}_j^{n+1} = \overline{\rho}_j^n + \lambda \left(v_{j-\frac{1}{2}} h(\rho_{j-\frac{1}{2}}^-, \rho_{j-\frac{1}{2}}^+) - v_{j+\frac{1}{2}} h(\rho_{j+\frac{1}{2}}^-, \rho_{j+\frac{1}{2}}^+) \right), \tag{3.2}$$

The analysis in section 2.2 implies the following theorem.

Theorem 3.1 *Suppose the DG solution $\rho^n > 0$ in scheme (3.2), then under the CFL condition*

$$\max_j |v_{j-\frac{1}{2}}|\lambda < \alpha_0,$$

we have $\bar{\rho}^{n+1} > 0$.

The above theorem guarantees the positivity of the numerical cell averages. However, the numerical solutions (which are piecewise polynomials) might be negative at some points and we can modify the density ρ_j^n in the following steps.

- Set up a small number $\varepsilon = \min\left\{10^{-13}, \bar{\rho}_j^n\right\}$.
- Compute $m_j = \min_i \rho_j^n(x_i^j)$, where $\{x_i^j\}$ are the Gauss-Lobatto points in cell I_j.
- If $m_j < \varepsilon$, then we take

$$\theta = \frac{\overline{\rho}_j^n - \varepsilon}{\overline{\rho}_j^n - m_j},$$

  and use

$$\widetilde{\rho}_j^n = \overline{\rho}_j^n + \theta(\rho_j^n - \overline{\rho}_j^n) \tag{3.3}$$

  as the DG approximation in cell I_j at time level n.

Following the above steps, the numerical density is always positive. Therefore

$$\|\rho^n\|_{L^1(\Omega)} = \int_\Omega \rho^n(x)dx = \int_\Omega \rho^0(x)dx = \|\rho_0\|_{L^1(\Omega)}, \tag{3.4}$$

where $\|u\|_{L^1(\Omega)}$ is the standard L^1 norm of u on Ω. Clearly, (3.4) implies the L^1 stability for the DG scheme. Moreover, we can also derive a sufficient CFL condition which does not depend on the numerical velocity in Theorem 3.1. Actually, Notice the fact that

$$v_{j-\frac{1}{2}} = \sum_{i=1}^{N} \int_{I_i} (y - x_{j-\frac{1}{2}})\xi(y - x_{j-\frac{1}{2}})\rho_i^n(y)dy \le R\|\rho_0\|_{L^1(\Omega)},$$

the sufficient CFL condition is

$$\lambda \le \frac{\alpha_0}{R\|\rho_0\|_{L^1(\Omega)}}. \tag{3.5}$$

To sum up, we have the following theorem.

Theorem 3.2 *Under the CFL condition* (3.5)*, the DG scheme* (2.1) *with the positivity-preserving limiter for equation* (1.2) *is* L^1 *stable and the density function is always positive.*

3.2 Numerical experiments

In this subsection, some numerical examples will be given to demonstrate the good performance of the DG scheme.

Example 1. We consider the following problem

$$\begin{array}{ll} \rho_t + (v\rho)_x = 0, & x \in [0,1], t > 0, \\ \rho(x,0) = \rho_0(x), & t > 0, \end{array} \tag{3.6}$$

where the velocity v is defined by

$$v(x,t) = \int_{x-R}^{x+R} (y-x)\rho(y,t)dy.$$

We apply the positivity-preserving limiter and use $\mathcal{P}^0$ and $\mathcal{P}^1$ polynomials. Moreover, we use the third order SSP Runge-Kutta discretization in time [23] with $\Delta t = 0.1\Delta x$. Figure

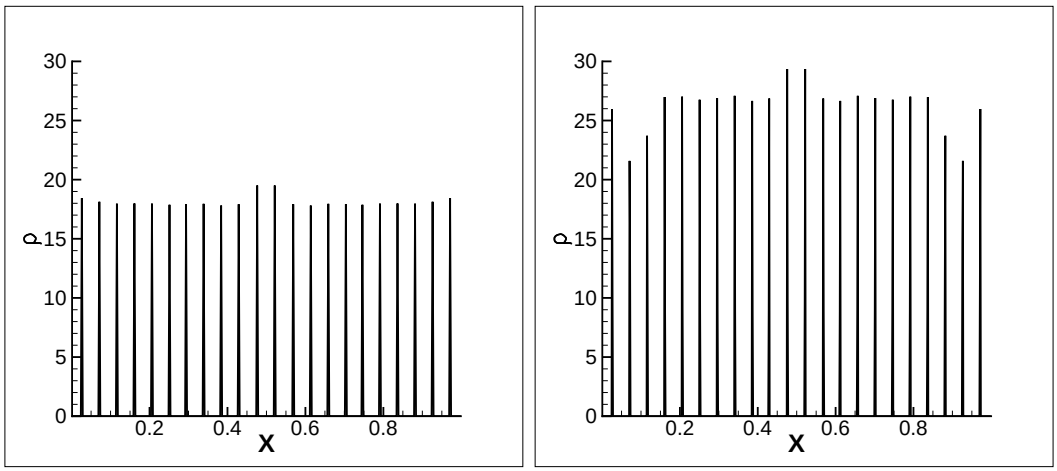

Figure 3.1: Numerical density for (3.6) at $t = 1000$ with positivity-preserving limiter when using $\mathcal{P}^0$ (left) and $\mathcal{P}^1$ (right) polynomials. Other parameters are taken to be CFL=0.1, N=400 and R=0.02.

3.1 shows the numerical approximations of $\rho(x)$ at $t = 1000$, with $N = 400$, $\rho_0 = 1$, and $R = 0.02$. We can observe 22 δ-singularities in each panel, and the distance between any two adjacent singularities is greater than R. Even though we perform a long time simulation,

the numerical solution does not blow up and the density is still positive. Therefore, the algorithm is quite stable in this simulation. Moreover, the $\mathcal{P}^1$ solution in the right panel is more accurate than the $\mathcal{P}^0$ one in the left panel, since the heights of the δ-singularities are almost doubled.

Example 2. We consider the model problem in two dimensions.

$$\begin{array}{ll} \rho_t + \mathrm{div}(\mathbf{v}\rho) = 0, & \mathbf{x} \in [-1,1]^2, t > 0, \\ \rho(\mathbf{x}, 0) = \rho_0(\mathbf{x}), & t > 0, \end{array} \tag{3.7}$$

where the velocity $\mathbf{v}$ is defined by

$$\mathbf{v}(\mathbf{x}, t) = \int_{B_R(\mathbf{x})} (\mathbf{y} - \mathbf{x}) \rho(\mathbf{y}, t) d\mathbf{y}.$$

In this example, we take $R = 0.1$ and

$$\rho_0(\mathbf{x}) = \begin{cases} 1 & r < 0.5, \\ 0 & r > 0.5, \end{cases}$$

where $r = \|\mathbf{x}\|$ is the Euclidean norm of $\mathbf{x}$. In [7], the authors demonstrated that the exact solution should be a single delta placed at the origin. However, by using rectangle meshes, we observe more than one delta singularity for R sufficiently small. This is because the meshes are not invariant under rotation. To tackle this problem, we follow the same ideas in [9, 10], and construct a special mesh, namely equal-angle-zoned mesh. The structure of the mesh is given in figure 3.2. By using such a special mesh, the limit density given in figure 3.3 is a single delta placed at the origin.

4 Pressureless Euler equations

In this section, we apply DG methods to pressureless Euler equations.

4.1 Numerical schemes in one dimension

We study equation (1.3) in one space dimension and consider the following system

$$\mathbf{w}_t + \mathbf{f}(\mathbf{w})_x = 0, \quad t > 0, x \in \mathbb{R}, \tag{4.1}$$

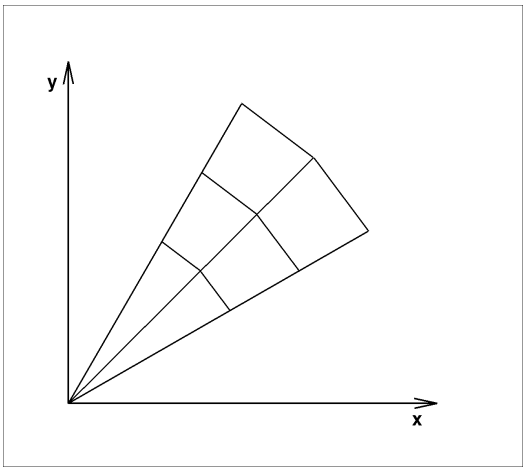

Figure 3.2: Equal-angle-zoned mesh.

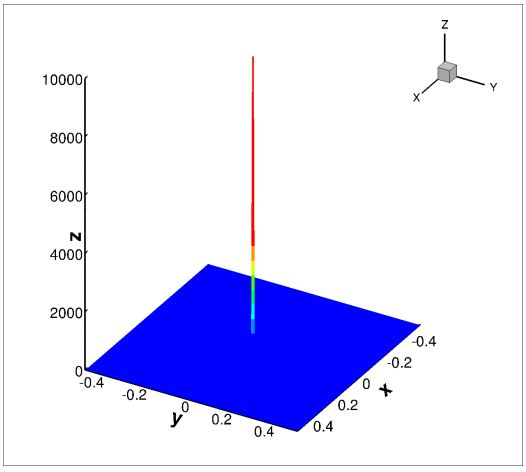

Figure 3.3: Numerical density ρ for (3.7) at $t = 2000$ with $N = 200$ when using $\mathcal{P}^0$ polynomials. Other parameters are taken to be CFL=0.2 and R=0.1.

$$\mathbf{w} = \begin{pmatrix} \rho \\ m \end{pmatrix}, \quad \mathbf{f}(\mathbf{w}) = \begin{pmatrix} m \\ \rho u^2 \end{pmatrix},$$

with $m = \rho u$, where ρ is the density function and u is the velocity. Physically, the density is positive and the velocity satisfies the maximum principle. Therefore, we define

$$G = \left\{ \mathbf{w} = \begin{pmatrix} \rho \\ m \end{pmatrix} : \rho > 0, a\rho \le m \le b\rho \right\},$$

where

$$a = \min u_0(x), \qquad b = \max u_0(x), \tag{4.2}$$

with u_0 being the initial velocity. Clearly, G is a convex set.

4.1.1 First order scheme

Following the same analysis in section 2.2, we start with the first order scheme,

$$\mathbf{w}_j^{n+1} = \mathbf{w}_j^n + \lambda \left(\mathbf{h}(\mathbf{w}_{j-1}^n, \mathbf{w}_j^n) - \mathbf{h}(\mathbf{w}_j^n, \mathbf{w}_{j+1}^n) \right), \tag{4.3}$$

where $\mathbf{h}(\cdot,\cdot)$ is a numerical flux and $\mathbf{w}_j^n = \left(\rho_j^n, m_j^n\right)^T$ is the numerical approximation to the exact solution in cell I_j at time level n. Moreover, we define $\overline{\mathbf{w}}_j^n = \left(\overline{\rho}_j^n, \overline{m}_j^n\right)^T$ as its cell average. Clearly, for a first order scheme, $\mathbf{w}_j^n = \overline{\mathbf{w}}_j^n$ in (4.3). For simplicity, we use u_j^n for $\frac{m_j^n}{\rho_j^n}$ as the numerical velocity throughout this section. In this problem, we consider the Godunov flux [4]. Suppose at the cell interface $x = x_{j-\frac{1}{2}}$ we have two numerical approximations $\mathbf{w}_\ell = (\rho_\ell, m_\ell)^T$ and $\mathbf{w}_r = (\rho_r, m_r)^T$ from left and right respectively. Then the Godunov flux is given as

$$\left(\mathbf{h}\left(\mathbf{w}_\ell, \mathbf{w}_r\right)\right)^T = \left(\widehat{\rho u}_{j-\frac{1}{2}}, \widehat{\rho u^2}_{j-\frac{1}{2}}\right) = \begin{cases} (m_\ell, \rho_\ell u_\ell^2) & u_\ell > 0, u_r > 0, \\ (0,0) & u_\ell \le 0, u_r > 0, \\ (m_r, \rho_r u_r^2) & u_\ell \le 0, u_r \le 0, \\ (m_\ell, \rho_\ell u_\ell^2) & u_\ell > 0, u_r \le 0, v > 0, \\ (m_r, \rho_r u_r^2) & u_\ell > 0, u_r \le 0, v < 0, \\ (\frac{m_\ell + m_r}{2}, \rho_\ell u_\ell^2 = \rho_r u_r^2) & u_\ell > 0, u_r \le 0, v = 0, \end{cases} \tag{4.4}$$

where

$$u_\ell = \frac{m_\ell}{\rho_\ell}, \quad u_r = \frac{m_r}{\rho_r}, \text{ and } v = \frac{\sqrt{\rho_\ell} u_\ell + \sqrt{\rho_r} u_r}{\sqrt{\rho_\ell} + \sqrt{\rho_r}}.$$

For this problem, $\mathbf{H}_1$ and $\mathbf{H_2}$ are taken to be

$$\mathbf{H}_1(\mathbf{u},\mathbf{v},c) = \mathbf{v} + c\,\mathbf{h}(\mathbf{u},\mathbf{v}), \quad \mathbf{H_2}(\mathbf{u},\mathbf{v},c) = \mathbf{u} - c\,\mathbf{h}(\mathbf{u},\mathbf{v}). \tag{4.5}$$

Clearly, the scheme (4.3) can be written as

$$\mathbf{w}_j^{n+1} = \frac{1}{2}\mathbf{H}_1\left(\mathbf{w}_{j-1}^n, \mathbf{w}_j^n, 2\lambda\right) + \frac{1}{2}\mathbf{H}_2\left(\mathbf{w}_j^n, \mathbf{w}_{j+1}^n, 2\lambda\right).$$

Before proceeding to the theoretical results for the scheme above, we would like to introduce the following lemma, whose proof is trivial and is omitted.

Lemma 4.1 *Suppose $\{x_i\}$ are positive real numbers, and $a \le y_i \le b, \forall i$, then*

$$a \le \frac{\sum_{i=1}^n x_i y_i}{\sum_{i=1}^n x_i} \le b.$$

We will use Lemma 4.1 to prove the following lemma.

Lemma 4.2 *Assume $\mathbf{w}^n \in G$ in scheme (4.3), then under the CFL condition*

$$\lambda < \frac{1}{2\max(|a|,|b|)},$$

where a and b are defined in (4.2), we have $\mathbf{w}^{n+1} \in G$.

Proof: We will only prove $\mathbf{H}_1\left(\mathbf{w}_{j-1}^n, \mathbf{w}_j^n, 2\lambda\right) \in G$ and the proof for $\mathbf{H}_2\left(\mathbf{w}_j^n, \mathbf{w}_{j+1}^n, 2\lambda\right) \in G$ follows the same lines. Define $\mathbf{H}_1\left(\mathbf{w}_{j-1}^n, \mathbf{w}_j^n, 2\lambda\right) = (\check{\rho}, \check{m})^T$, then the velocity derived from $\mathbf{H}_1$ is given as

$$\check{u} = \frac{\check{m}}{\check{\rho}} = \frac{m_j^n + 2\lambda\widehat{\rho u^2}_{j-\frac{1}{2}}}{\rho_j^n + 2\lambda\widehat{\rho u}_{j-\frac{1}{2}}}. \tag{4.6}$$

We will prove $\check{\rho} > 0$ and $a \le \check{u} \le b$. To do so, we have to determine what $\{x_i\}$ and $\{y_i\}$ should be in Lemma 4.1, by testing the different choices for the numerical flux in (4.4). For simplicity, we define $\widehat{u}_{j-\frac{1}{2}} = \frac{\widehat{\rho u^2}_{j-\frac{1}{2}}}{\widehat{\rho u}_{j-\frac{1}{2}}}$, if $\widehat{\rho u}_{j-\frac{1}{2}} \neq 0$.

- If $\widehat{\rho u}_{j-\frac{1}{2}} = m_{j-1}^n$, then $\widehat{u}_{j-\frac{1}{2}} = u_{j-1}^n > 0$. We take $x_1 = \rho_j^n$, $y_1 = u_j^n$ and $x_2 = 2\lambda m_{j-1}^n$, $y_2 = u_{j-1}^n$.

- If $\widehat{\rho u}_{j-\frac{1}{2}} = m_j^n$, then $\widehat{u}_{j-\frac{1}{2}} = u_j^n \le 0$. We take $x_1 = \rho_j^n + 2\lambda m_j^n$, $y_1 = u_j^n$.

- If $\widehat{\rho u}_{j-\frac{1}{2}} = (m^n_{j-1} + m^n_j)/2$, then $\widehat{\rho u^2}_{j-\frac{1}{2}} = (m^n_{j-1}u^n_{j-1} + m^n_j u^n_j)/2$. We combine the two situations above, and take $x_1 = \rho^n_j + \lambda m^n_j$, $y_1 = u^n_j$ and $x_2 = \lambda m^n_{j-1}$, $y_2 = u^n_{j-1}$.

- If $\widehat{\rho u}_{j-\frac{1}{2}} = 0$, then $\widehat{\rho u^2}_{j-\frac{1}{2}} = 0$. We take $x_1 = \rho^n_j$, $y_1 = u^n_j$.

Clearly, in each case, $x_i > 0$, therefore $\check{\rho} > 0$. Moreover, we observe $a \le y_i \le b$, then by Lemma 4.1, we have $a \le \check{u} \le b$. □

4.1.2 High order scheme

Now, we move on to high order schemes and consider the numerical cell averages which satisfy the following equation

$$\overline{\mathbf{w}}^{n+1}_j = \overline{\mathbf{w}}^n_j + \lambda \left(\mathbf{h}(\mathbf{w}^-_{j-\frac{1}{2}}, \mathbf{w}^+_{j-\frac{1}{2}}) - \mathbf{h}(\mathbf{w}^-_{j+\frac{1}{2}}, \mathbf{w}^+_{j+\frac{1}{2}}) \right), \tag{4.7}$$

By the same analysis as in section 2.2, we have the following theorem.

Theorem 4.1 *Under the CFL condition*

$$\lambda < \frac{\alpha_0}{\max(|a|, |b|)},$$

$\mathbf{w}^n \in G$ *in scheme* (4.7)*implies* $\overline{\mathbf{w}}^{n+1} \in G$.

From the above theorem, we can obtain desired numerical cell average which is in G. Many cases, the numerical solution $\mathbf{w}^n_j$ may not be in the target set. Then we modify the numerical solution while keeping the cell average untouched. Due to the rounding error, we define

$$G^\varepsilon = \left\{ \mathbf{w} = \begin{pmatrix} \rho \\ m \end{pmatrix} : \rho \ge \varepsilon, a - \varepsilon \le \frac{m}{\rho} \le b + \varepsilon \right\},$$
$$\partial G^\varepsilon = \left\{ \mathbf{w} = \begin{pmatrix} \rho \\ m \end{pmatrix} : \rho \ge \varepsilon, \frac{m}{\rho} = a - \varepsilon \text{ or } b + \varepsilon \right\}.$$

Then the modification of $\mathbf{w}^n_j$ is given in the following steps.

- Set up a small number $\varepsilon = 10^{-13}$.

- If $\bar{\rho}_j^n > \varepsilon$, then proceed to the following steps. Otherwise, ρ_j^n is identified as the approximation to vacuum, and the velocity is undefined. Therefore, we take $\widetilde{\mathbf{w}}_j^n = \overline{\mathbf{w}}_j^n$ as the numerical solution and skip the following steps.

- Modify the density first: Compute $m_j = \min_i \rho_j^n(x_i^j)$, where $\{x_i^j\}$ are the Gauss-Lobatto points in cell I_j, and get $\widetilde{\rho}_j^n$ by (3.3). Then use $\widetilde{\rho}_j^n$ as the new numerical density ρ_j^n.

- Modify the velocity: Define $\mathbf{q}_i^j = \mathbf{w}_j^n(x_i^j)$ in cell I_j. If $\mathbf{q}_i^j \in G^\varepsilon$, then take $\theta_i^j = 1$. Otherwise, take

$$\theta_i^j = \frac{\left\|\overline{\mathbf{w}}_j^n - \mathbf{s}_i^j\right\|}{\left\|\overline{\mathbf{w}}_j^n - \mathbf{q}_i^j\right\|},$$

where $\|\cdot\|$ is the Euclidean norm, and $\mathbf{s}_i^j$ is the intersection point of the straight line

$$\mathbf{s}(t) = (1-t)\overline{\mathbf{w}}_j^n + t\mathbf{q}_i^j, \quad 0 \le t \le 1,$$

and the surface ∂G^ε. Define $\theta_j = \min_{i=0,\cdots,m} \theta_i^j$, and use

$$\widetilde{\mathbf{w}}_j^n = \overline{\mathbf{w}}_j^n + \theta_j(\mathbf{w}_j^n - \overline{\mathbf{w}}_j^n),$$

as the DG approximation in cell I_j.

4.2 Numerical schemes in two dimensions

We extend our work to two dimensions and study the following equation

$$\mathbf{w}_t + \mathbf{f}(\mathbf{w})_x + \mathbf{g}(\mathbf{w})_y = 0, \quad t > 0,\ (x,y) \in \mathbb{R}^2, \tag{4.8}$$

$$\mathbf{w} = \begin{pmatrix} \rho \\ m \\ n \end{pmatrix}, \quad \mathbf{f}(\mathbf{w}) = \begin{pmatrix} m \\ \rho u^2 \\ \rho uv \end{pmatrix}, \quad \mathbf{g}(\mathbf{w}) = \begin{pmatrix} n \\ \rho uv \\ \rho v^2 \end{pmatrix},$$

with

$$m = \rho u, \quad n = \rho v,$$

where ρ is the density function and (u, v) is the velocity field. We define

$$G = \left\{ \mathbf{w} = \begin{pmatrix} \rho \\ m \\ n \end{pmatrix} : \rho > 0, m^2 + n^2 \le S^2\rho^2 \right\},$$

where

$$S > 0, \text{ and } S^2 = \max_{x,y} \left(u^2(x,y,0) + v^2(x,y,0)\right)$$

with $(u,v)(x,y,0)$ being the initial velocity field. Clearly, G is a convex set.

For simplicity, we use uniform rectangular meshes. The cell is defined as $I_{ij} = \left[x_{i-\frac{1}{2}}, x_{i+\frac{1}{2}}\right] \times \left[y_{j-\frac{1}{2}}, y_{j+\frac{1}{2}}\right]$, and the mesh sizes in x and y directions are denoted as Δx and Δy respectively. At time level n, we approximate the exact solution with a vector of polynomials of degree k, $\mathbf{w}_{ij}^n = (\rho_{ij}^n, m_{ij}^n, n_{ij}^n)^T$, and define the cell average $\overline{\mathbf{w}}_{ij}^n = (\overline{\rho}_{ij}^n, \overline{m}_{ij}^n, \overline{n}_{ij}^n)^T$. Moreover, we denote $\mathbf{w}^+_{i-\frac{1}{2},j}(y), \mathbf{w}^-_{i+\frac{1}{2},j}(y), \mathbf{w}^+_{i,j-\frac{1}{2}}(x), \mathbf{w}^-_{i,j+\frac{1}{2}}(x)$ as the traces of $\mathbf{w}$ on the four edges in cell I_{ij} respectively. More details can be found in [26]. In this subsection, we always use (u_{ij}^n, v_{ij}^n) for $(\frac{m_{ij}^n}{\rho_{ij}^n}, \frac{n_{ij}^n}{\rho_{ij}^n})$ as the numerical velocity field in cell I_{ij} at time level n, and define $a_1 = \max_{ij} |u_{ij}^n|$ and $a_2 = \max_{ij} |v_{ij}^n|$. For simplicity, if we consider a generic numerical solution on the whole computational domain at time level n, then the subscript ij will be omitted.

In this section, we only consider high order schemes, and the one satisfied by the cell averages can be written as

$$\begin{aligned}\overline{\mathbf{w}}_{ij}^{n+1} = \overline{\mathbf{w}}_{ij}^n &+ \frac{\Delta t}{\Delta x \Delta y} \int_{y_{j-\frac{1}{2}}}^{y_{j+\frac{1}{2}}} \mathbf{h}_1\left(\mathbf{w}^-_{i-\frac{1}{2},j}(y), \mathbf{w}^+_{i-\frac{1}{2},j}(y)\right) - \mathbf{h}_1\left(\mathbf{w}^-_{i+\frac{1}{2},j}(y), \mathbf{w}^+_{i+\frac{1}{2},j}(y)\right) dy \\ &+ \frac{\Delta t}{\Delta x \Delta y} \int_{x_{i-\frac{1}{2}}}^{x_{i+\frac{1}{2}}} \mathbf{h}_2\left(\mathbf{w}^-_{i,j-\frac{1}{2}}(x), \mathbf{w}^+_{i,j-\frac{1}{2}}(x)\right) - \mathbf{h}_2\left(\mathbf{w}^-_{i,j+\frac{1}{2}}(x), \mathbf{w}^+_{i,j+\frac{1}{2}}(x)\right) dx, \end{aligned} \tag{4.9}$$

where $\mathbf{h}_1(\cdot,\cdot)$ and $\mathbf{h}_2(\cdot,\cdot)$ are one-dimensional numerical fluxes. For this problem, we also use the Godunov flux. Suppose $(x,y) = (x_{i-\frac{1}{2}}, y_0)$ is a point on the vertical cell interface, at which we have two numerical approximations $\mathbf{w}_\ell = (\rho_\ell, m_\ell, n_\ell)^T$ and $\mathbf{w}_r = (\rho_r, m_r, n_r)^T$ from left and right respectively. Then the Godunov flux $(\mathbf{h}_1(\mathbf{w}_\ell, \mathbf{w}_r))^T$ can be written as

$$\left(\widehat{\rho u}, \widehat{\rho u^2}, \widehat{\rho uv}\right) = \begin{cases} (m_\ell, \rho_\ell u_\ell^2, \rho_\ell u_\ell v_\ell) & u_\ell > 0, u_r > 0, \\ (0,0,0) & u_\ell \le 0, u_r > 0, \\ (m_r, \rho_r u_r^2, \rho_r u_r v_r) & u_\ell \le 0, u_r \le 0, \\ (m_\ell, \rho_\ell u_\ell^2, \rho_\ell u_\ell v_\ell) & u_\ell > 0, u_r \le 0, v > 0, \\ (m_r, \rho_r u_r^2, \rho_r u_r v_r) & u_\ell > 0, u_r \le 0, v < 0, \\ \frac{1}{2}(m_\ell + m_r, \rho_\ell u_\ell^2 + \rho_r u_r^2, m_\ell v_\ell + m_r v_r) & u_\ell > 0, u_r \le 0, v = 0, \end{cases}$$

where

$$(u_\ell, v_\ell) = \left(\frac{m_\ell}{\rho_\ell}, \frac{n_\ell}{\rho_\ell}\right), \ (u_r, v_r) = \left(\frac{m_r}{\rho_r}, \frac{n_\ell}{\rho_\ell}\right), \text{ and } v = \frac{\sqrt{\rho_\ell} u_\ell + \sqrt{\rho_r} u_r}{\sqrt{\rho_\ell} + \sqrt{\rho_r}}.$$

The numerical flux $\mathbf{h}_2 = \left(\widehat{\rho v}, \widehat{\rho uv}, \widehat{\rho v^2}\right)^T$ can be defined in a similar way on the horizontal cell interfaces.

For accuracy, we use L-point Gauss quadratures with $L \geq k+1$ to approximate the integrals in (4.9). More details of this requirement can be found in [12]. The Gauss quadrature points on $\left[x_{i-\frac{1}{2}}, x_{i+\frac{1}{2}}\right]$ and $\left[y_{j-\frac{1}{2}}, y_{j+\frac{1}{2}}\right]$ are denoted by

$$p_i^x = \left\{x_i^\beta : \beta = 1, \cdots, L\right\} \text{ and } p_j^y = \left\{y_j^\beta : \beta = 1, \cdots, L\right\},$$

respectively. Also, we denote w_β as the corresponding weights on the interval $\left[-\frac{1}{2}, \frac{1}{2}\right]$. Different from the notations in previous sections, we use

$$\hat{p}_i^x = \{\hat{x}_i^\alpha : \alpha = 0, \cdots, M\} \text{ and } \hat{p}_j^y = \left\{\hat{y}_j^\alpha : \alpha = 0, \cdots, M\right\}$$

as the Gauss-Lobatto points on $\left[x_{i-\frac{1}{2}}, x_{i+\frac{1}{2}}\right]$ and $\left[y_{j-\frac{1}{2}}, y_{j+\frac{1}{2}}\right]$ respectively. Also, we denote $\hat{w}_\alpha$ as the corresponding weights on the interval $\left[-\frac{1}{2}, \frac{1}{2}\right]$.

Let $\lambda_1 = \frac{\Delta t}{\Delta x}$ and $\lambda_2 = \frac{\Delta t}{\Delta y}$, then the numerical scheme (4.9) becomes

$$\begin{aligned}\overline{\mathbf{w}}_{ij}^{n+1} = \overline{\mathbf{w}}_{ij}^n &+ \lambda_1 \sum_{\beta=1}^{L} w_\beta \left[\mathbf{h}_1\left(\mathbf{w}_{i-\frac{1}{2},\beta}^-, \mathbf{w}_{i-\frac{1}{2},\beta}^+\right) - \mathbf{h}_1\left(\mathbf{w}_{i+\frac{1}{2},\beta}^-, \mathbf{w}_{i+\frac{1}{2},\beta}^+\right)\right] \\ &+ \lambda_2 \sum_{\beta=1}^{L} w_\beta \left[\mathbf{h}_2\left(\mathbf{w}_{\beta,j-\frac{1}{2}}^-, \mathbf{w}_{\beta,j-\frac{1}{2}}^+\right) - \mathbf{h}_2\left(\mathbf{w}_{\beta,j+\frac{1}{2}}^-, \mathbf{w}_{\beta,j+\frac{1}{2}}^+\right)\right], \end{aligned} \tag{4.10}$$

where $\mathbf{w}_{i-\frac{1}{2},\beta}^- = \mathbf{w}_{i-\frac{1}{2},j}^-(y_j^\beta)$ is a point value in the Gauss quadrature. Likewise for the other point values. As the general treatment, we rewrite the cell average on the right hand side as

$$\overline{\mathbf{w}}_{ij}^n = \sum_{\alpha=0}^{M}\sum_{\beta=1}^{L} \hat{w}_\alpha w_\beta \mathbf{w}_{\alpha\beta}^1 = \sum_{\alpha=0}^{M}\sum_{\beta=1}^{L} \hat{w}_\alpha w_\beta \mathbf{w}_{\beta\alpha}^2,$$

where $\mathbf{w}_{\alpha\beta}^1$ and $\mathbf{w}_{\beta\alpha}^2$ denote $\mathbf{w}_{ij}^n(\hat{x}_i^\alpha, y_j^\beta)$ and $\mathbf{w}_{ij}^n(x_i^\beta, \hat{y}_j^\alpha)$ respectively. We extend the definitions of $\mathbf{H}_1$ and $\mathbf{H}_2$ in (4.5) to two-dimensional problems and define

$$\begin{aligned}\mathbf{H}_1^1(\mathbf{u}, \mathbf{v}, c) &= \mathbf{v} + c\,\mathbf{h}_1(\mathbf{u}, \mathbf{v}), \quad \mathbf{H}_2^1(\mathbf{u}, \mathbf{v}, c) = \mathbf{u} - c\,\mathbf{h}_1(\mathbf{u}, \mathbf{v}), \\ \mathbf{H}_1^2(\mathbf{u}, \mathbf{v}, c) &= \mathbf{v} + c\,\mathbf{h}_2(\mathbf{u}, \mathbf{v}), \quad \mathbf{H}_2^2(\mathbf{u}, \mathbf{v}, c) = \mathbf{u} - c\,\mathbf{h}_2(\mathbf{u}, \mathbf{v}).\end{aligned}$$

Let $\mu = a_1\lambda_1 + a_2\lambda_2$, then scheme (4.10) can be written as

$$\begin{aligned}\overline{\mathbf{w}}_{ij}^{n+1} = {} & C_1 \sum_{\beta=1}^{L} w_\beta \left(\sum_{\alpha=1}^{M-1} \hat{w}_\alpha \mathbf{w}_{\alpha\beta}^1 + \hat{w}_0 \mathbf{H}_1^1 \left(\mathbf{w}_{i-\frac{1}{2},\beta}^-, \mathbf{w}_{i-\frac{1}{2},\beta}^+, \mu_1 \right) + \hat{w}_M \mathbf{H}_2^1 \left(\mathbf{w}_{i+\frac{1}{2},\beta}^-, \mathbf{w}_{i+\frac{1}{2},\beta}^+, \mu_1 \right) \right) \\ & + C_2 \sum_{\beta=1}^{L} w_\beta \left(\sum_{\alpha=1}^{M-1} \hat{w}_\alpha \mathbf{w}_{\beta\alpha}^2 + \hat{w}_0 \mathbf{H}_1^2 \left(\mathbf{w}_{\beta,j-\frac{1}{2}}^-, \mathbf{w}_{\beta,j-\frac{1}{2}}^+, \mu_2 \right) + \hat{w}_M \mathbf{H}_2^2 \left(\mathbf{w}_{\beta,i+\frac{1}{2}}^-, \mathbf{w}_{\beta,j+\frac{1}{2}}^+, \mu_2 \right) \right),\end{aligned}$$

where

$$C_1 = \frac{a_1\lambda_1}{\mu},\ C_2 = \frac{a_2\lambda_2}{\mu},\ \mu_1 = \frac{\mu}{a_1\hat{w}_0},\ \mu_2 = \frac{\mu}{a_2\hat{w}_0}.$$

Now, we can state the main theorem.

Theorem 4.2 *Suppose* $\mathbf{w}^n \in G$ *in scheme* (4.10)*, then under the CFL condition*

$$\frac{\Delta t}{\Delta x} a_1 + \frac{\Delta t}{\Delta y} a_2 \le \hat{w}_0,$$

we have $\overline{\mathbf{w}}^{n+1} \in G$.

Proof: For simplicity, we only prove $\mathbf{H}_1^1 \left(\mathbf{w}_{i-\frac{1}{2},\beta}^-, \mathbf{w}_{i-\frac{1}{2},\beta}^+, \mu_1 \right) \in G, \forall \beta$, and define

$$\mathbf{H}_1^1 \left(\mathbf{w}_{i-\frac{1}{2},\beta}^-, \mathbf{w}_{i-\frac{1}{2},\beta}^+, \mu_1 \right) = (\check{\rho}, \check{m}, \check{n})^T, \check{u} = \frac{\check{m}}{\check{\rho}}, \check{v} = \frac{\check{n}}{\check{\rho}}.$$

Following the same analysis as in Lemma 4.2, we have $\check{\rho} > 0$. Therefore, we need only prove $\check{u}^2 + \check{v}^2 \le S^2$. By the assumption, we have

$$\mathbf{w}_{i-\frac{1}{2},\beta}^- = \left(\rho_{i-\frac{1}{2},\beta}^-, m_{i-\frac{1}{2},\beta}^-, n_{i-\frac{1}{2},\beta}^- \right)^T \in G \text{ and } \mathbf{w}_{i-\frac{1}{2},\beta}^+ = \left(\rho_{i-\frac{1}{2},\beta}^+, m_{i-\frac{1}{2},\beta}^+, n_{i-\frac{1}{2},\beta}^+ \right)^T \in G.$$

Denote $\mathbf{h}_1 \left(\mathbf{w}_{i-\frac{1}{2},\beta}^-, \mathbf{w}_{i-\frac{1}{2},\beta}^+ \right) = \left(\widehat{\rho u}_{i-\frac{1}{2},\beta}, \widehat{\rho u^2}_{i-\frac{1}{2},\beta}, \widehat{\rho uv}_{i-\frac{1}{2},\beta} \right)^T$ as the corresponding numerical flux, and for any unit vector $\mathbf{n} = (n_1, n_2)^T$, define $\check{w} = \check{u}n_1 + \check{v}n_2$. Then

$$\begin{aligned}\check{w} &= \frac{m_{i-\frac{1}{2},\beta}^+ n_1 + n_{i-\frac{1}{2},\beta}^+ n_2 + \mu_1 \left(\widehat{\rho u^2}_{i-\frac{1}{2},\beta} n_1 + \widehat{\rho uv}_{i-\frac{1}{2},\beta} n_2 \right)}{\rho_{i-\frac{1}{2},\beta}^+ + \mu_1 \widehat{\rho u}_{i-\frac{1}{2},\beta}} \\ &= \frac{\rho_{i-\frac{1}{2},\beta}^+ w_{i-\frac{1}{2},\beta}^+ + \mu_1 \widehat{\rho u}_{i-\frac{1}{2},\beta} \widehat{w}_{i-\frac{1}{2},\beta}}{\rho_{i-\frac{1}{2},\beta}^+ + \mu_1 \widehat{\rho u}_{i-\frac{1}{2},\beta}},\end{aligned}$$

where

$$w_{i-\frac{1}{2},\beta}^+ = \frac{m_{i-\frac{1}{2},\beta}^+ n_1 + n_{i-\frac{1}{2},\beta}^+ n_2}{\rho_{i-\frac{1}{2},\beta}^+}, \quad \widehat{w}_{i-\frac{1}{2},\beta} = \frac{\widehat{\rho u^2}_{i-\frac{1}{2},\beta} n_1 + \widehat{\rho uv}_{i-\frac{1}{2},\beta} n_2}{\widehat{\rho u}_{i-\frac{1}{2},\beta}}.$$

We can easily show that $|w^+_{i-\frac{1}{2},\beta}| \le S$ and $|\widehat{w}_{i-\frac{1}{2},\beta}| \le S$. Following the same lines as the proof of Lemma 4.2, we have $|\check{w}| \le S$. Especially, choosing $\mathbf{n}$ to be parallel with $(\check{u}, \check{v})$, we have $\check{u}^2 + \check{v}^2 \le S^2$, completing the proof. □

Remark 4.1 *Since $a_1 \le S$ and $a_2 \le S$, another sufficient CFL condition in Theorem 4.2 is* $\frac{\Delta t}{\Delta x} + \frac{\Delta t}{\Delta y} \le \frac{\hat{w}_0}{S}$.

Based on the above theorem, the numerical cell average we obtained is in G. Unfortunately, the numerical solution $\mathbf{w}^n_{ij}$ might be placed outside. Hence, we have to modify the numerical solution while keeping the cell average untouched. Due to the rounding error, we define

$$G^\varepsilon = \left\{ \mathbf{w} = \begin{pmatrix} \rho \\ m \\ n \end{pmatrix} : \rho \ge \varepsilon, m^2 + n^2 \le (S+\varepsilon)^2 \rho^2 \right\},$$

$$\partial G^\varepsilon = \left\{ \mathbf{w} = \begin{pmatrix} \rho \\ m \\ n \end{pmatrix} : \rho \ge \varepsilon, m^2 + n^2 = (S+\varepsilon)^2 \rho^2 \right\}.$$

Then the modification of $\mathbf{w}^n_{ij}$ is given in the following steps.

- Set up a small number $\varepsilon = 10^{-13}$.
- If $\overline{\rho}^n_{ij} > \varepsilon$, then proceed to the following steps. Otherwise, ρ^n_{ij} is identified as the approximation to vacuum, and the velocity is undefined. Therefore, we take $\widetilde{\mathbf{w}}^n_{ij} = \overline{\mathbf{w}}^n_{ij}$ as the numerical solution and skip the following steps.
- Modify the density first: Compute $m_{ij} = \min_{\alpha\beta} \left\{ \rho^n_{ij}(\widehat{x}^\alpha_i, y^\beta_j), \rho^n_{ij}(x^\beta_i, \widehat{y}^\alpha_j) \right\}$. If $m_{ij} < \varepsilon$, then take $\widetilde{\rho}^n_{ij}$ as

  $$\widetilde{\rho}^n_{ij} = \overline{\rho}^n_{ij} + \theta_{ij} \left(\rho^n_{ij} - \overline{\rho}^n_{ij} \right),$$

  with

  $$\theta_{ij} = \frac{\overline{\rho}^n_{ij} - \varepsilon}{\overline{\rho}^n_{ij} - m_{ij}},$$

  and use $\widetilde{\rho}^n_{ij}$ as the new numerical density ρ^n_{ij}.

- Modify the velocity: Consider $\mathbf{w}^1_{\alpha\beta}$ and $\mathbf{w}^2_{\beta\alpha}$ in cell I_{ij} respectively. If $\mathbf{w}^1_{\alpha\beta} \in G^\varepsilon$, then take $\theta^1_{\alpha\beta} = 1$. Otherwise, take

$$\theta^1_{\alpha\beta} = \frac{\left\|\overline{\mathbf{w}}^n_{ij} - \mathbf{s}^1_{\alpha\beta}\right\|}{\left\|\overline{\mathbf{w}}^n_{ij} - \mathbf{w}^1_{\alpha\beta}\right\|},$$

where $\|\cdot\|$ is the Euclidean norm, and $\mathbf{s}^1_{\alpha\beta}$ is the intersection point of the straight line

$$\mathbf{s}^1(t) = (1-t)\overline{\mathbf{w}}^n_{ij} + t\mathbf{w}^1_{\alpha\beta}, \quad 0 \le t \le 1,$$

and the surface ∂G^ε. Similarly, we can define $\theta^2_{\beta\alpha}$ in the same way for $\mathbf{w}^2_{\beta\alpha}$. Finally, we use

$$\widetilde{\mathbf{w}}^n_{ij} = \overline{\mathbf{w}}^n_{ij} + \theta(\mathbf{w}^n_{ij} - \overline{\mathbf{w}}^n_{ij}), \quad \theta = \min_{\alpha,\beta}\left\{\theta^1_{\alpha\beta}, \theta^2_{\beta\alpha}\right\},$$

as the DG approximation in cell I_{ij}.

4.3 Numerical experiments

In this subsection, we provide numerical experiments to demonstrate the good performance of the DG scheme for solving pressureless Euler equations. In all the numerical simulations, if not otherwise stated, we use third order schemes and take $N = 100$.

4.3.1 One space dimension

We consider the problem in one space dimension and solve equation (4.1) with different initial conditions.

Example 1. We consider the following initial data

$$\rho_0(x) = sin(x) + 2, \ u_0(x) = \sin(x) + 2, \tag{4.11}$$

with periodic boundary condition. Clearly, the exact solution is

$$u(x,t) = u_0(x_0), \quad \rho(x,t) = \frac{\rho_0(x_0)}{1 + u_0'(x_0)},$$

where x_0 is given implicitly by

$$x_0 + tu_0(x_0) = x.$$

We use the third order SSP multi-step method in time [22] with $\Delta t = 0.01\Delta x^2$, and test the example by using $\mathcal{P}^k$ polynomials with $k = 1, 2, 3$ on uniform meshes. Table 4.1, shows the L^2-norm of the error at $t = 0.1$. We observe $(k + 0.5)$-th order convergence.

Table 4.1: L^2-norm of the error between the numerical density and the exact density for (4.1) with initial condition (4.11).

	k=1		k=2		k=3	
N	error	order	error	order	error	order
20	1.41E-02	-	6.84E-04	-	3.40e-5	-
40	4.18E-03	1.76	1.04E-04	2.72	2.82e-6	3.59
80	1.30E-03	1.68	1.55E-05	2.74	2.26e-7	3.64
160	4.24E-04	1.62	2.41E-06	2.69	1.83e-8	3.62
320	1.51E-04	1.49	3.80E-07	2.67	1.49e-9	3.63

Example 2. We consider the following initial condition

$$\rho_0(x) = \begin{cases} 1 & x < 0, \\ 0.25 & x > 0, \end{cases} \qquad u_0(x) = \begin{cases} 1 & x < 0, \\ 0 & x > 0. \end{cases} \tag{4.12}$$

Clearly, the exact solution is

$$(\rho(x,t), u(x,t)) = \begin{cases} (1,1) & x < 2t/3, \\ (0.25, 0) & x > 2t/3, \end{cases}$$

and at $x = \frac{2t}{3}$, the density should be a δ-function. Figure 4.1 shows the numerical density and velocity at $t = 0.5$ with $\mathcal{P}^1$ polynomials and bound-preserving limiter. Without such limiter, the density and velocity blows up immediately. From the figure, we observe the numerical solution capture the profile of the exact solution quite well and the velocity keeps bounded. Therefore, the limiter is good in approximating δ-functions and controlling the velocity .

Example 3. We consider the following initial condition

$$\rho_0(x) = 0.5, \quad u_0(x) = \begin{cases} -0.5 & x < -0.5, \\ 0.4 & -0.5 < x < 0, \\ 0.4 - x & 0 < x < 0.8, \\ -0.4 & x > 0.8, \end{cases} \tag{4.13}$$

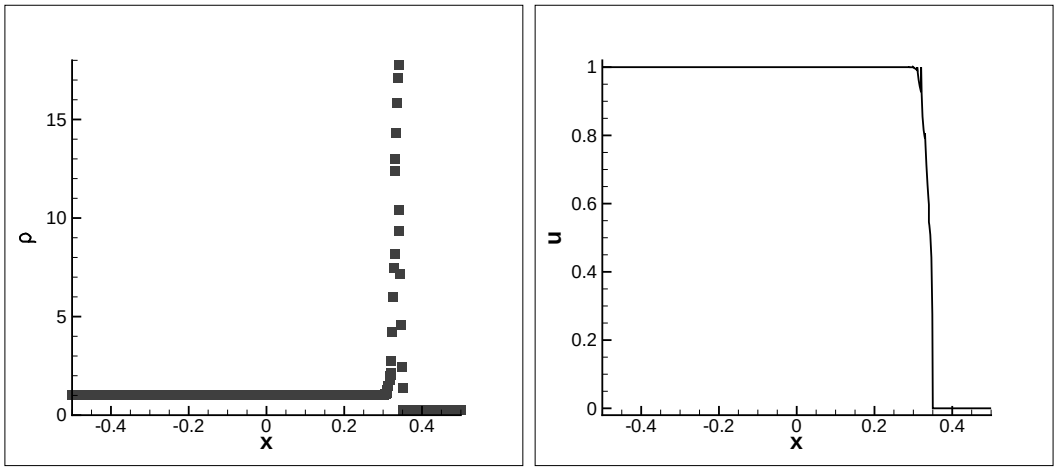

Figure 4.1: Numerical density (left) and velocity (right) at $t = 0.5$ with $\mathcal{P}^1$ polynomials and bound-preserving limiter for (4.1) with initial condition (4.12). Other parameters are taken to be $N = 100$, CFL=0.01 and $\varepsilon = 10^{-13}$.

and the exact solution for $t < 1$ is

$$(\rho(x,t), u(x,t)) = \begin{cases} (0.5, -0.5) & x < -0.5 - 0.5t, \\ (0, \text{undefined}) & -0.5 - 0.5t < x < -0.5 + 0.4t, \\ (0.5, 0.4) & -0.5 + 0.4t < x < 0.4t, \\ (\frac{0.5}{1-t}, \frac{0.4-x}{1-t}) & 0.4t < x < 0.8 - 0.4t, \\ (0.5, -0.4) & x > 0.8 - 0.4t. \end{cases}$$

Figure 4.2 shows the numerical density and velocity at $t = 0.5$. From the figure, we can observe some local oscillations near the singularities. This is not surprising as we have not used any limiters other than the bound-preserving ones for the DG scheme.

Example 4. We consider the following initial condition

$$\rho_0(x) = 0.5, \quad u_0(x) = \begin{cases} -0.5 & x < 0, \\ 0.4 & x > 0, \end{cases} \tag{4.14}$$

and the exact solution is

$$(\rho(x,t), u(x,t)) = \begin{cases} (0.5, -0.5) & x < -0.5t, \\ (0, \text{undefined}) & -0.5t < x < 0.4t, \\ (0.5, 0.4) & x > 0.4t. \end{cases}$$

Figure 4.3 shows the numerical density and velocity at $t = 0.5$. We use $\mathcal{P}^2$ polynomials and bound-preserving limiter only, therefore, we can observe some local oscillations near the singularities. This example demonstrates that the bound-preserving DG method is also

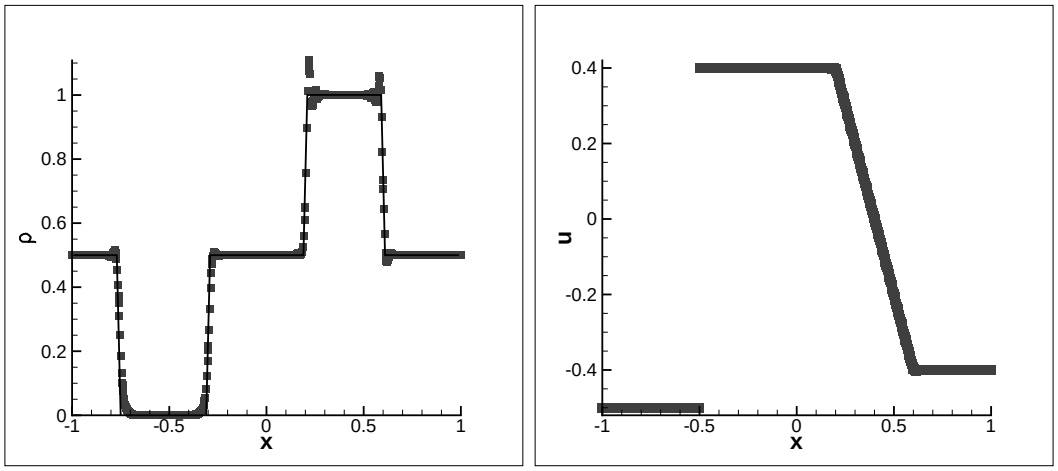

Figure 4.2: Numerical density (left) and velocity (right) at $t = 0.5$ with $\mathcal{P}^2$ polynomials and bound-preserving limiter for (4.1) with initial condition (4.13). The solid line shows the exact solution while the symbols show the numerical solution. Other parameters are taken to be $N = 100$, CFL=0.01 and $\varepsilon = 10^{-13}$.

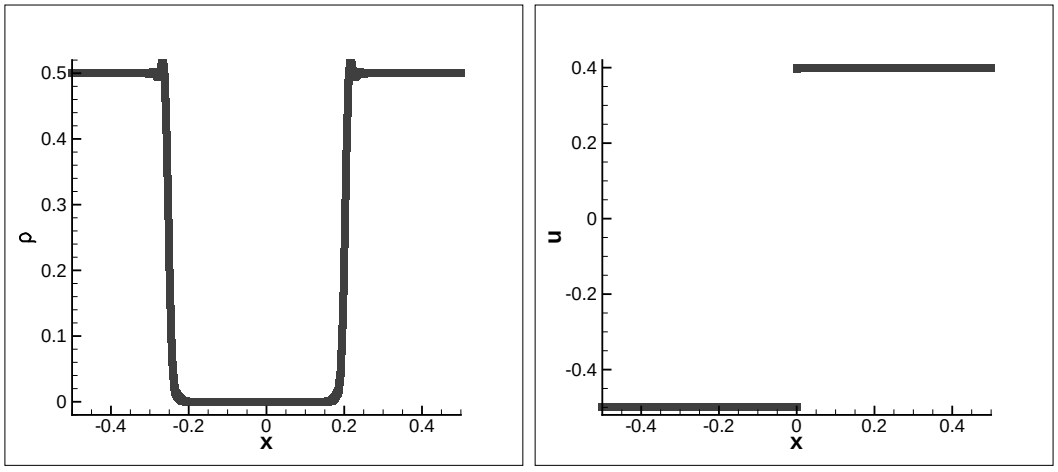

Figure 4.3: Numerical density (left) and velocity (right) at $t = 0.5$ with $\mathcal{P}^2$ polynomials and bound-preserving limiter for (4.1) with initial condition (4.14). Other parameters are taken to be $N = 100$, CFL=0.01 and $\varepsilon = 10^{-13}$.

good for approximations in the presence of vacuum, and the limiter keeps the density to be positive.

4.3.2 Two dimensions

We consider the problem in two dimensions and solve equation (4.8) with different initial conditions.

Example 1. We consider the following initial condition

$$\begin{aligned} \rho(x,y,0) &= \rho_0(x+y) = \exp(\sin(x+y)), \\ u(x,y,0) &= u_0(x+y) = \tfrac{1}{3}(\cos(x+y)+2), \\ v(x,y,0) &= v_0(x+y) = \tfrac{1}{3}(\sin(x+y)+2). \end{aligned} \tag{4.15}$$

The exact solution is

$$u(x,y,t) = u_0(z_0), \quad v(x,y,t) = v_0(z_0), \quad \rho(x,y,t) = \frac{\rho_0(z_0)}{1+u_0'(z_0)+v_0'(z_0)},$$

where z_0 is given implicitly by

$$z_0 + t(u_0(z_0)+v_0(z_0)) = x+y.$$

We use the third order SSP multi-step method in time [22] with $\Delta t = 0.01\Delta x^{3/2}$, and test the example by using $\mathcal{P}^k$ polynomials with $k = 1,2,3$. Table 4.2 shows the L^2-norm of the error at $t = 0.1$. From the table, we again observe about $(k+0.5)$-th order convergence.

Table 4.2: L^2-norm of the error between the numerical density and the exact density for (4.8) with initial condition (4.15).

	k=1		k=2		k=3	
N	error	order	error	order	error	order
10	0.512	-	0.107	-	3.42E-02	-
20	0.176	1.54	3.12E-02	1.78	3.57E-03	3.26
40	6.48E-02	1.44	8.52E-03	1.87	4.86E-04	2.88
80	2.32E-02	1.48	1.39E-03	2.62	3.97E-05	3.61
160	9.08E-03	1.35	1.92E-04	2.86	3.65E-06	3.45

Example 2. We consider the following initial condition

$$\rho(x,y,0)=\frac{1}{100},\quad (u,v)(x,y,0)=(-\frac{1}{10}\cos\theta,-\frac{1}{10}\sin\theta), \tag{4.16}$$

where θ is the polar angle. Since all the particles are moving towards the origin, the density

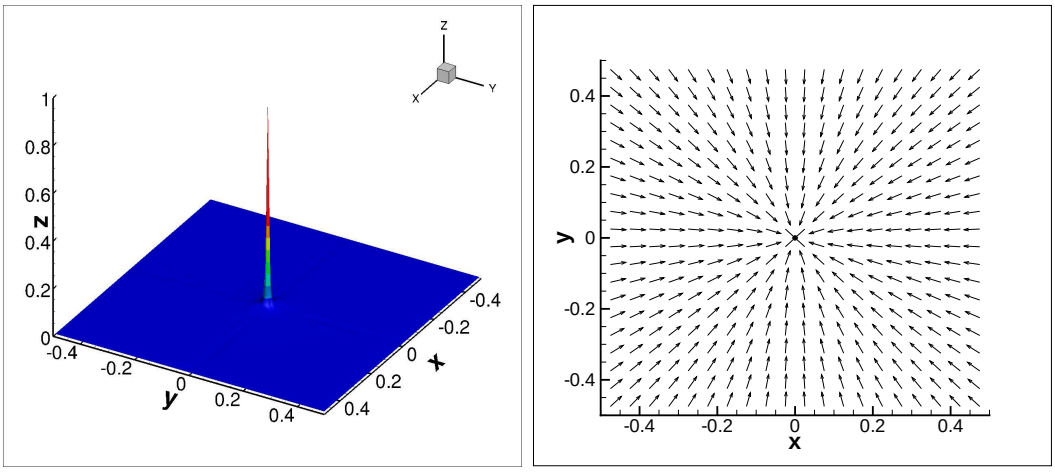

Figure 4.4: Numerical density (left) and velocity field (right) at $t=0.5$ with $\mathcal{P}^2$ polynomials and bound-preserving limiter for (4.8) with initial condition (4.16). Other parameters are taken to be $N=100$, CFL=0.01 and $\varepsilon=10^{-13}$.

function at $t>0$ should be a single delta at the origin. Different from example 2 in section 3.2, we can observe only one delta located at the origin by using rectangle mesh and the result is given in figure 4.4.

Example 3. We consider the following initial condition

$$\rho(x,y,0)=\frac{1}{10},\quad (u,v)(x,y,0)=\begin{cases}(-0.25,-0.25) & x>0,y>0,\\ (0.25,-0.25) & x<0,y>0,\\ (0.25,0.25) & x<0,y<0,\\ (-0.25,0.25) & x>0,y<0.\end{cases} \tag{4.17}$$

Figure 4.5 shows the numerical density and velocity field at $t=0.5$. The velocity, pointing towards the center, keeps a constant in each quadrant, therefore, we can observe δ-singularities located at the origin and two axes.

Example 4. We consider the following initial condition

$$\rho(x,y,0)=\frac{1}{100},\quad (u,v)(x,y,0)=\begin{cases}(\cos\theta,\sin\theta) & r<0.3,\\ (-\frac{1}{2}\cos\theta,-\frac{1}{2}\sin\theta) & r>0.3,\end{cases} \tag{4.18}$$

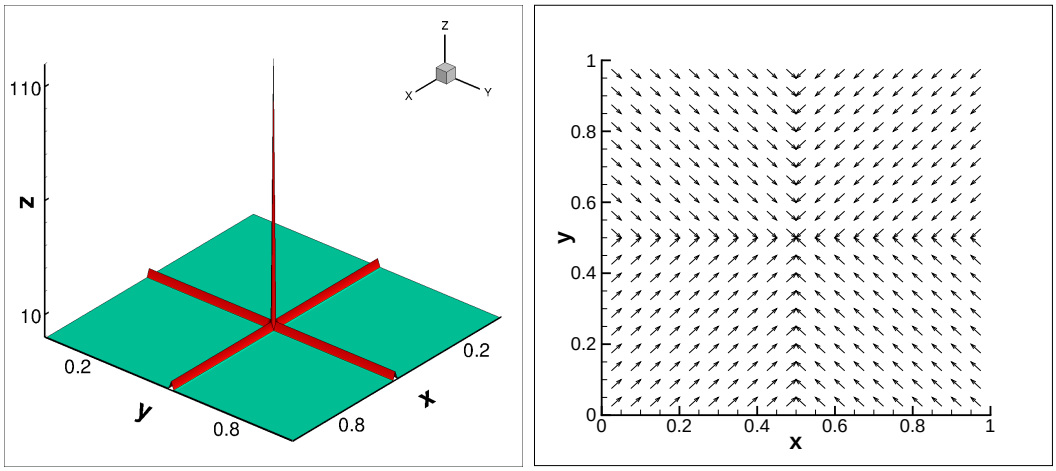

Figure 4.5: Numerical density (left) and velocity field (right) at $t = 0.5$ with $\mathcal{P}^2$ polynomials and bound-preserving limiter for (4.8) with initial condition (4.17). Other parameters are taken to be $N = 100$, CFL=0.01 and $\varepsilon = 10^{-13}$.

where $r = \sqrt{x^2 + y^2}$ and θ is the polar angle. Figure 4.6 shows the numerical density

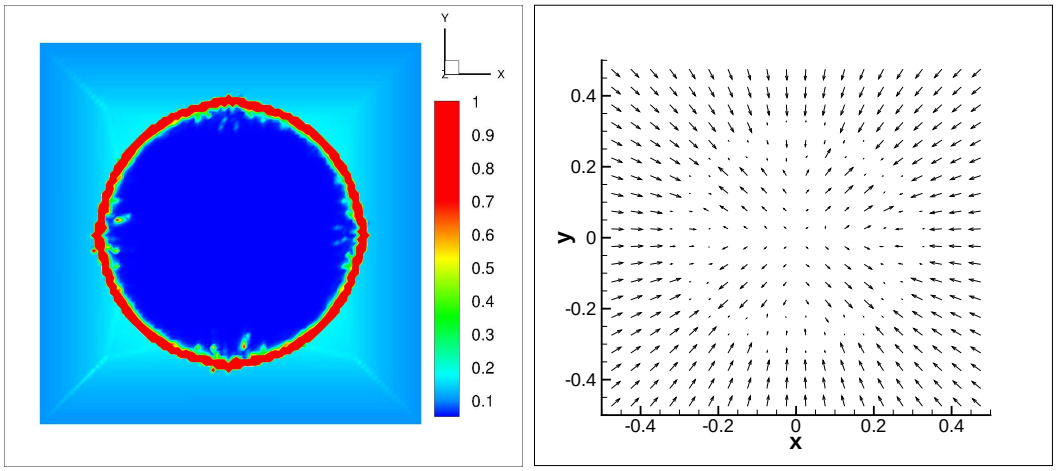

Figure 4.6: Numerical density (left) and velocity field (right) at $t = 0.5$ with $\mathcal{P}^2$ polynomials and bound-preserving limiter for (4.8) with initial condition (4.18). Other parameters are taken to be $N = 100$, CFL=0.01 and $\varepsilon = 10^{-13}$.

(contour plot) and velocity field at $t = 0.5$. From the figure, we can observe δ-shocks located on a circle and vacuum inside. In this example, we also use third order DG method with bound-preserving limiter, therefore, some local oscillations are placed near the δ-shocks. Since the problem contains vacuum, we have to use bound-preserving limiter to keep the

positivity of the density.

Example 5. We consider the following initial condition

$$\rho(x,y,0)=0.5,\quad (u,v)(x,y,0)=\begin{cases}(0.3,0.4) & x>0,y>0,\\ (-0.4,0.3) & x<0,y>0,\\ (-0.3,-0.4) & x<0,y<0,\\ (0.4,-0.3) & x>0,y<0.\end{cases} \tag{4.19}$$

Figure 4.7 shows the numerical density (contour plot) and velocity field with $N = 50$ at

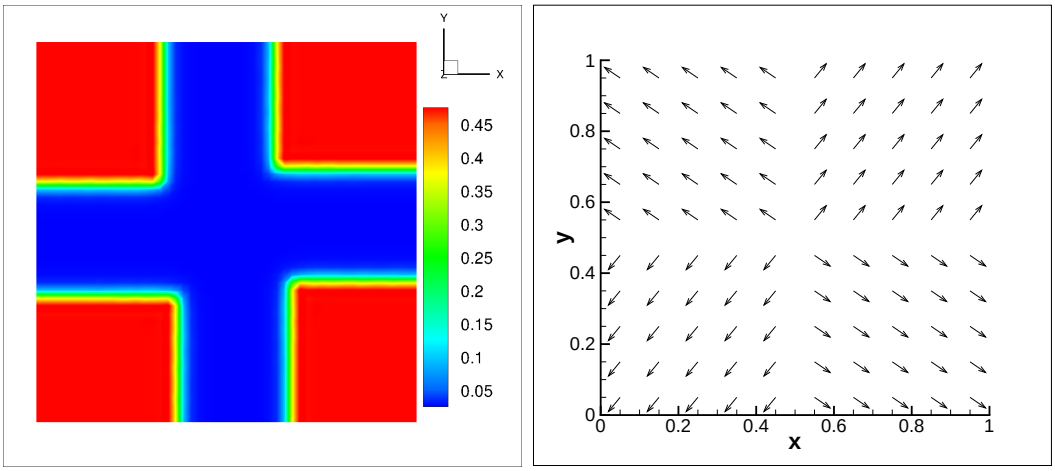

Figure 4.7: Numerical density (left) and velocity field (right) at $t = 0.1$ with $\mathcal{P}^2$ polynomials and bound-preserving limiter for (4.8) with initial condition (4.19). Other parameters are taken to be $N = 50$, CFL=0.01 and $\varepsilon = 10^{-13}$.

$t = 0.1$. From the figure, we can observe that the numerical solution approximates the vacuum quite well. Because of the presence of vacuum, the boundary-preserving limiter is used to avoid negative density.

5 Concluding remarks

In this paper, we apply discontinuous Galerkin (DG) method to solve hyperbolic conservation laws involving δ-singularities. We study Krause's consensus models and pressureless Euler equations to demonstrate the stability and high resolution of the DG approximations. Moreover, numerical experiments show that the scheme is also good for approximations in

the presence of vacuum. In future work we will extend DG methods to other equations involving δ-singularities in wider areas of applications.

References

[1] C. Berthon, M. Breuss and M.-O. Titeux, *A relaxation scheme for the approximation of the pressureless Euler equations*, Numerical Methods for Partial Differential Equations, 22, (2006), 484-505.

[2] F. Bouchut, *On zero pressure gas dynamics*, Advances in Kinetic Theory and Computing, Would Scientific, River Edge, NJ, 1994, 171-190.

[3] F. Bouchut and F. James, *Duality solutions for pressureless gases, monotone scalar conservation laws, and uniqueness*, Communications in Partial Differential Equations, 24, (1999), 2173-2189.

[4] F. Bouchut, S. Jin and X. Li, *Numerical approximations of pressureless and isothermal gas dynamics*, SIAM Journal on Numerical Analysis, 41, (2003), 135-158.

[5] L. Boudin and J. Mathiaud, *A numerical scheme for the one-dimensional pressureless gases system*, Numerical Methods for Partial Differential Equations, 28, (2006), 1729-1746.

[6] Y. Brenier and E. Grenier, *Sticky particles and scalar conservation laws*, SIAM Journal on Numerical Analysis, 35, (1998), 2317-2328.

[7] C. Canuto, F. Fagnani and P. Tilli, *An Eulerian approach to the analysis of Krause's consensus models*, SIAM Journal on Control and Optimization, 50, (2012), 243-265.

[8] G.-Q. Chen and H. Liu, *Formation of δ-shocks and vacuum states in the vanishing pressure limit of solutions to the Euler equations for isentropic fluids*, SIAM Journal on Mathematical Analysis, 34, (2003), 925-938.

[9] J. Cheng and C.-W. Shu, *A cell-centered Lagrangian scheme with the preservation of symmetry and conservation properties for compressible fluid flows in two-dimensional cylindrical geometry*, Journal of Computational Physics, 229, (2010), 7191-7206.

[10] J. Cheng and C.-W. Shu, *Improvement on spherical symmetry in two-dimensional cylindrical coordinates for a class of control volume Lagrangian schemes*, Communications in Computational Physics, 11, (2012), 1144-1168.

[11] A. Chertock, A. Kurganov and Y. Rykov, *A new sticky particle method for pressureless gas dynamics*, SIAM Journal on Numerical Analysis, 45, (2007), 2408-2441.

[12] B. Cockburn, S. Hou and C.-W. Shu, *The Runge-Kutta local projection discontinuous Galerkin finite element method for conservation laws IV: the multidimensional case*, Mathematics of Computation, 54 (1990), 545-581.

[13] B. Cockburn, S.-Y. Lin and C.-W. Shu, *TVB Runge-Kutta local projection discontinuous Galerkin finite element method for conservation laws III: one-dimensional systems*, Journal of Computational Physics, 84 (1989), 90-113.

[14] B. Cockburn and C.-W. Shu, *TVB Runge-Kutta local projection discontinuous Galerkin finite element method for conservation laws II: general framework*, Mathematics of Computation, 52 (1989), 411-435.

[15] B. Cockburn and C.-W. Shu, *The Runge-Kutta discontinuous Galerkin method for conservation laws V: multidimensional systems*, Journal of Computational Physics, 141 (1998), 199-224.

[16] W. E., Yu. G. Rykov and Ya. G. Sinai, *Generalized variational principles, global weak solutions and behavior with random initial data for systems of conservation laws arising in adhesion particle dynamics*, Communications in Mathematical Physics, 177 (1996), 349-380.

[17] S. Gottlieb, C.-W. Shu and E. Tadmor, *Strong stability-preserving high-order time discretization methods*, SIAM Review, 43 (2001), 89-112.

[18] C. Johnson and J. Pitkäranta, *An analysis of the discontinuous Galerkin method for a scalar hyperbolic equation*, Mathematics of Computation, 46 (1986), 1-26.

[19] W.H. Reed and T.R. Hill, *Triangular mesh methods for the Neutron transport equation*, Los Alamos Scientific Laboratory Report LA-UR-73-479, Los Alamos, NM, 1973.

[20] Yu. G. Rykov, *Propagation of shock wave type singularities in equations of two-dimensional zero-pressure gas dynamics*, Mathematical Notes, 66 (1999), 628-635.

[21] Yu. G. Rykov, *On the nonhamiltonian character of shocks in 2-D pressureless gas*, Bollettino della Unione Matematica Italiana. Serie VIII. Sezione B. Articoli di Ricerca Matematica, 5 (2002), 55-78.

[22] C.-W. Shu, *Total-variation-diminishing time discretizations*, SIAM Journal on Scientific and Statistical Computing, 9 (1988), 1073-1084.

[23] C.-W. Shu and S. Osher, *Efficient implementation of essentially non-oscillatory shock-capturing schemes*, Journal of Computational Physics, 77 (1988), 439-471.

[24] Y. Yang and C.-W. Shu, *Discontinuous Galerkin method for hyperbolic equations involving δ-singularities: negative-order norm error estimates and applications*, Numerische Mathematik, to appear. DOI 10.1007/s00211-013-0526-8.

[25] X. Zhang and C.-W. Shu, *On maximum-principle-satisfying high order schemes for scalar conservation laws*, Journal of Computational Physics, 229 (2010), 3091-3120.

[26] X. Zhang and C.-W. Shu, *On positivity preserving high order discontinuous Galerkin schemes for compressible Euler equations on rectangular meshes*, Journal of Computational Physics, 229 (2010), 8918-8934.

[27] X. Zhang and C.-W. Shu, *Maximum-principle-satisfying and positivity-preserving high order schemes for conservation laws: Survey and new developments*, Proceedings of the Royal Society A, 467 (2011), 2752-2776.

[28] X. Zhang and C.-W. Shu, *A minimum entropy principle of high order schemes for gas dynamics equations*, Numerische Mathematik, 121 (2012), 545-563.